Inorganic Chemistry

Article

pubs.acs.org/IC

Deprotonation in Mixed-Valent Diiron(II,III) Complexes with Aniline or Benzimidazole Ligands

Eric Gouré,[†,#] Michaël Carboni,[†,▽] Angélique Troussier,[†,‡] Patrick Dubourdeaux,[†] Martin Clémancey,[†,§] Nathalie Gon,[†,‡] Ramachandran Balasubramanian,[†,‡] Colette Lebrun,[∥,⊥] Jacques Pécaut,[∥,⊥] Geneviève Blondin,*[,†,‡] and Jean-Marc Latour*[,†]

[†]CEA, iRTSV-LCBM-pmb, 17 rue des Martyrs, 38054 Grenoble, France

[‡]CNRS, iRTSV-LCBM-pmb, 17 rue des Martyrs, 38054 Grenoble, France

[§]Univ. Grenoble Alpes, iRTSV-LCBM-pmb, 17 rue des Martyrs, 38054 Grenoble, France

[∥]CEA, INAC-SCIB-RICC, 38054 Grenoble, France

[⊥]Univ. Grenoble Alpes, INAC-SCIB-RICC, 38054 Grenoble, France

Supporting Information

ABSTRACT: We have previously investigated cis/trans isomerization processes in phenoxido-bridged mixed-valent $Fe^{II}Fe^{III}$ complexes that contain either one aniline or one anilide ligand. In this work, we compare the properties of similar complexes bearing one terminal protic ligand, either aniline or 1*H*-benzimidazole. Whatever the ligand, ^{1}H NMR spectroscopy clearly evidences that the complexes are present in CH_3CN as a mixture of cis- and trans-isomers in a close to 1:1 ratio. We show here that addition of NEt_3 indeed allows the deprotonation of these ligands, the resulting complexes bearing either anilide or benzimidazolide that are coordinated to the ferric site. The latter are singular examples of a high-spin ferric ion coordinated to a benzimidazolide ligand. Whereas the trans-isomer of the anilide complex is the overwhelming species, benzimidazolide species are mixtures of cis- and trans-isomers in equal proportions. Moreover, cyclic voltammametry studies show that $Fe^{III}Fe^{III}$ complexes with 1*H*-benzimidazole are more stable than their aniline counterparts, whereas the reverse is observed for the deprotonated species.

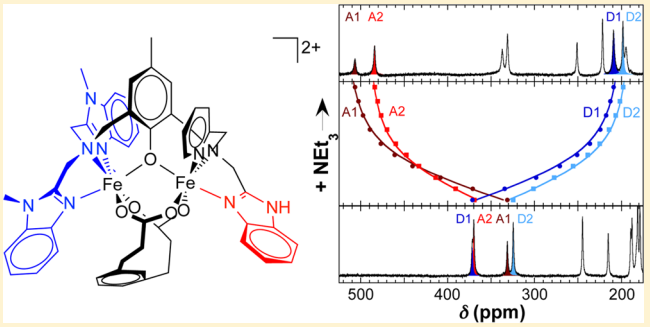

INTRODUCTION

Intervalence charge transfer (IVCT) has attracted continuous interest among inorganic chemists for several decades.[1] In most cases, it occurs through a ligand bridging two metals in different oxidation states, these metals being identical or not.[2−5] We recently reported that such an IVCT can be induced in a mixed-valent $Fe_2^{II,III}$ complex **1** by deprotonation of an aniline ligand bound to the ferrous site,[6] as illustrated in Scheme 1.

A similar process has been described only in an heterodinuclear RuOs complex[7] and in the semimet forms of the dioxygen carrier hemerythrin, albeit in the latter case the system switches between a ferrous pentacoordinate site and a hydroxo-bound hexacoordinate ferric center.[8] The thermodynamic and kinetic aspects of the deprotonation of **1** were investigated by spectroscopic and electrochemical techniques. A thorough electrochemical study of its redox properties and H/D labeling experiments have revealed that the deprotonation-induced intervalence transfer is indeed a concerted proton−electron transfer.[9] Owing to the peculiarity of this system, it appeared of interest to assess how the redox potentials of the iron centers and the acidity of the protic ligand influence this reaction. The modularity of the ligand constitution and its sequential synthesis[10] allow the variation of the complexing branch of each metal (see Chart 1). In this work, three complexes analogous to **1** and further denoted as **5**, **6**, and **7** were investigated (Scheme 2). The protic ligand is either the aniline group in **5** as in **1** or 1*H*-benzimidazole in **6** and **7**. When embedded in a bridging ligand, the protonation state of 1*H*-benzimidazole was shown to influence the metal−metal interactions.[11−13] 1*H*-Benzimidazole groups may also act as terminal ligands in dinuclear iron complexes.[14,15] It is proposed that the protonation state of one histidine in the Rieske protein is responsible for the shuttle of the iron−sulfur protein between the two cytochromes in the bacterial cytochrome *bc* complex.[16] The choice of 1*H*-benzimidazole was dictated here by the remote position of the exchangeable proton compared to that of aniline. The other branch of the binucleating ligand is either the *N*,*N*-bis((pyridin-2-yl)methyl)amine (BPA) in **6** as in **1** or the *N*,*N*-bis((1-methylbenzimidazol-2-yl)methyl)amine (BMBA) in **5** and **7**. In addition, the two iron ions are bridged by the dicarboxylato ligand *m*-phenylenedipropionate. Com-

Received: February 27, 2015
Published: June 19, 2015

DOI: 10.1021/acs.inorgchem.5b00449
Inorg. Chem. 2015, 54, 6257−6266

Scheme 1. Valence Inversion in the cis- and trans-Isomers of the $Fe^{II}Fe^{III}$ Complex 1 Resulting from Deprotonation of the Aniline Ligand

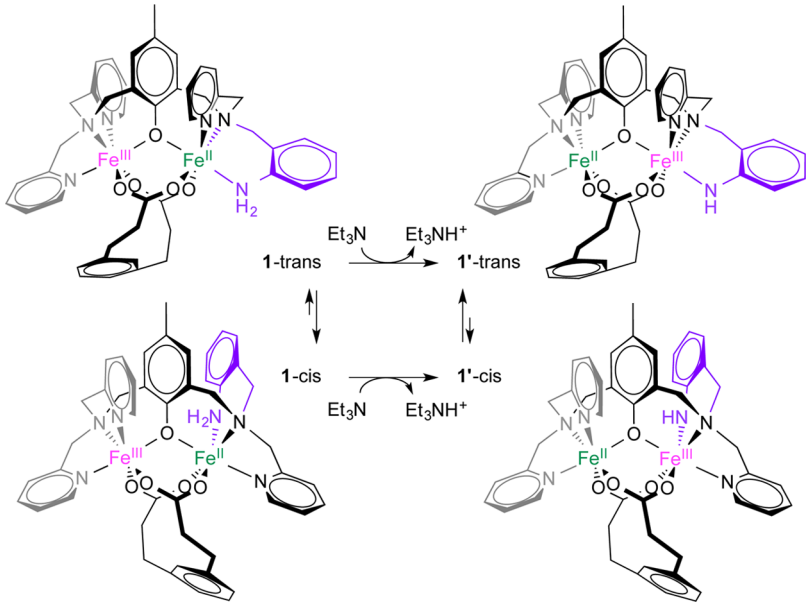

Chart 1. Scheme of the Ligands Used in This Work[a]

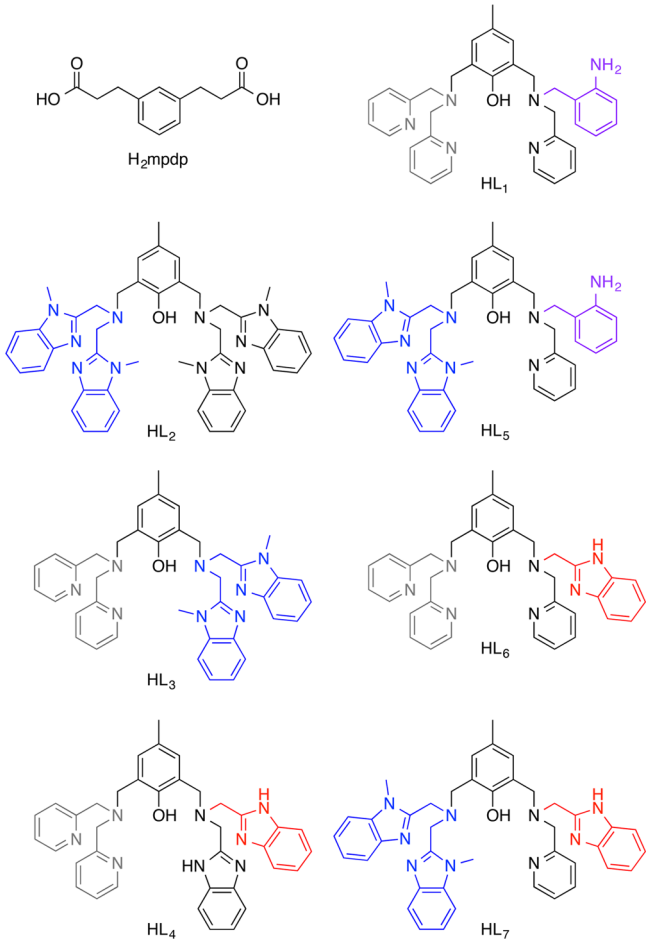

[a]The subscripts refer to the labels of the complexes.

Scheme 2. Six Dicationic Mixed-Valent $Fe_2^{II,III}$ Complexes 2–7 Investigated in This Work

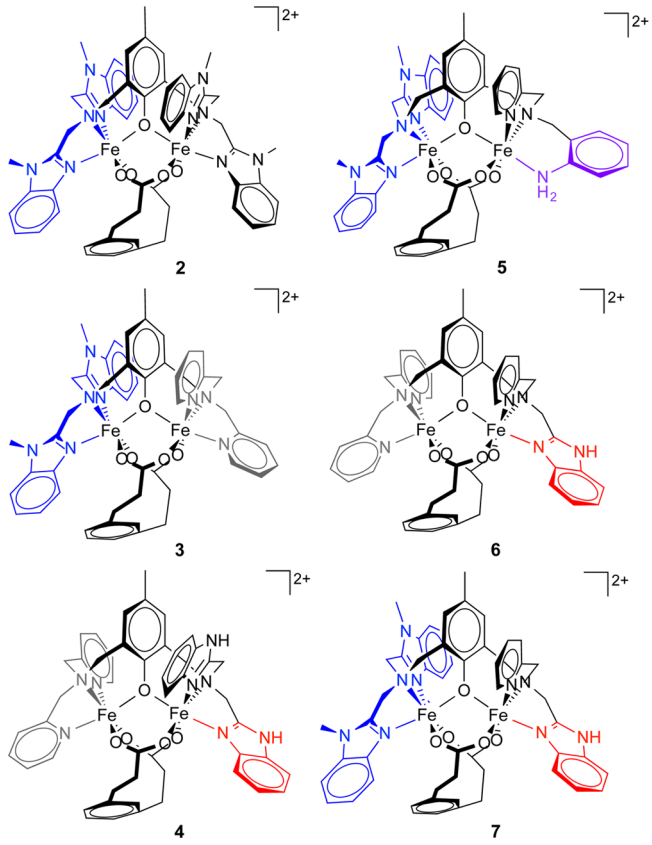

plexes **2**, **3**, and **4** were also synthesized for the sake of comparison (Scheme 2). We will show here that addition of triethylamine indeed leads to the deprotonation of the aniline ligand in **5** or the 1*H*-benzimidazole ligand in **4**, **6**, and **7**, the resulting anilide, or benzimidazolide being coordinated to the Fe^{III} ion.

We have recently evidenced by a combination of NMR, Mössbauer, and optical spectroscopies supported by DFT

DOI: 10.1021/acs.inorgchem.5b00449
Inorg. Chem. 2015, 54, 6257–6266

calculations that the aniline coordinated to the Fe^{II} ion in **1** and the anilide coordinated to the Fe^{III} in **1′** may be in trans or cis position with respect to the bridging phenoxide (see Scheme 1).[17] Moreover, the cis/trans ratios are different for the two complexes, ca. 65:35 in **1** and ca. 15:85 in **1′**, indicating that the trans-isomer of **1** is slightly more acidic than the cis-isomer. We will show here that similar isomers are present for complexes **5**−**7** as for the corresponding deprotonated species **6′** and **7′**.

RESULTS

Synthesis of the Ligands and Complexes. The ligands used in the present work (Chart 1) were synthesized according to the already published procedures that were adapted for inserting the desired *N*,*N*-bis((pyridin-2-yl)methyl)amine, *N*,*N*-bis((1-methylbenzimidazol-2-yl)methyl)amine, *N*,*N*-bis((1*H*-benzimidazol-2-yl)methyl)amine, *N*-((pyridin-2-yl)methyl)-*N*-((2-aminophenyl)methyl)amine, and *N*-((pyridin-2-yl)-methyl)-*N*-((1*H*-benzimidazol-2-yl)methyl)amine branches (see Supporting Information, Schemes S1 and S2). Complexes **2**−**7** were prepared by the usual procedures.[18,19] They were characterized by elemental analyses and ElectroSpray Ionization−Mass Spectroscopy (ESI-MS) and other spectroscopic techniques (see below).

X-ray Structures of $3(ClO_4)_2$ and $4(ClO_4)_2{\cdot}2CH_3CN$. Figure 1 displays the X-ray structure of the two dicationic complexes **3** and **4**. The crystal parameters are listed in Supporting Information, Table S1 and a selection of distances and angles in Supporting Information, Table S2. In both complexes, the two iron ions are bridged by the oxygen atom of the phenoxide of the deprotonated ditopic ligand and by the two carboxylates of *m*-phenylenedipropionate ($mpdp^{2-}$). The coordination spheres of the two metal ions are completed by three nitrogen atoms from one tertiary amine and two imines from the pyridine or the 1*H*- or 1-methylbenzimidazole groups. The overall N_3O_3 coordination around Fe1 and Fe2 corresponds to a rhombically distorted octahedron. The metal−ligand bond lengths compare well with those determined on similar complexes with either four pyridine groups as in $[(bpmp)Fe_2(\mu\text{-}OPr)_2]^{2+}$[20] or with four *N*-methylimidazole groups as in $[(bimp)Fe_2(\mu\text{-}O_2CPh)_2]^{2+}$.[21] The presence of the two perchlorate anions per diiron complex is in agreement with a mixed-valent $Fe^{II}Fe^{III}$ composition. Table 1 compares the Fe−O1 and the average Fe−ligand distances in the two complexes. In both systems, they are shorter for Fe2 than for Fe1, indicating that Fe1 is the ferrous site, while Fe2 is the ferric one. It must be noticed that in **3**, the Fe^{III} ion is in the BPA cavity, while the Fe^{II} ion is coordinated by the BMBA group. On the contrary, the BPA cavity in **4** is occupied by the Fe^{II} ion, the Fe^{III} being bound to the two 1*H*-benzimidazole groups. In addition, these groups are H-bonded with the perchlorate anions (see Supporting Information Figure S1), giving a slight benzimidazolide character to the ligands of Fe2 in **4**, further stabilizing its +III oxidation state. The valence locations are thus inverted in **3** and **4**. Because of the better donating character of the 1*H*- or 1-methylbenzimidazole compared to that of the pyridine, the valence location in **3** is counterintuitive and may result from solid state effects (see below).

^{1}H NMR Studies of Complexes 2−7. ^{1}H NMR spectra were recorded on CD_3CN solutions of complexes **2**−**5** and **7**; for complex **6**, a mixture of CD_3CN and d_7-DMF was used to ensure complete dissolution. They are shown in Supporting Information, Figure S2, and Figure 2 focuses on the 480−130

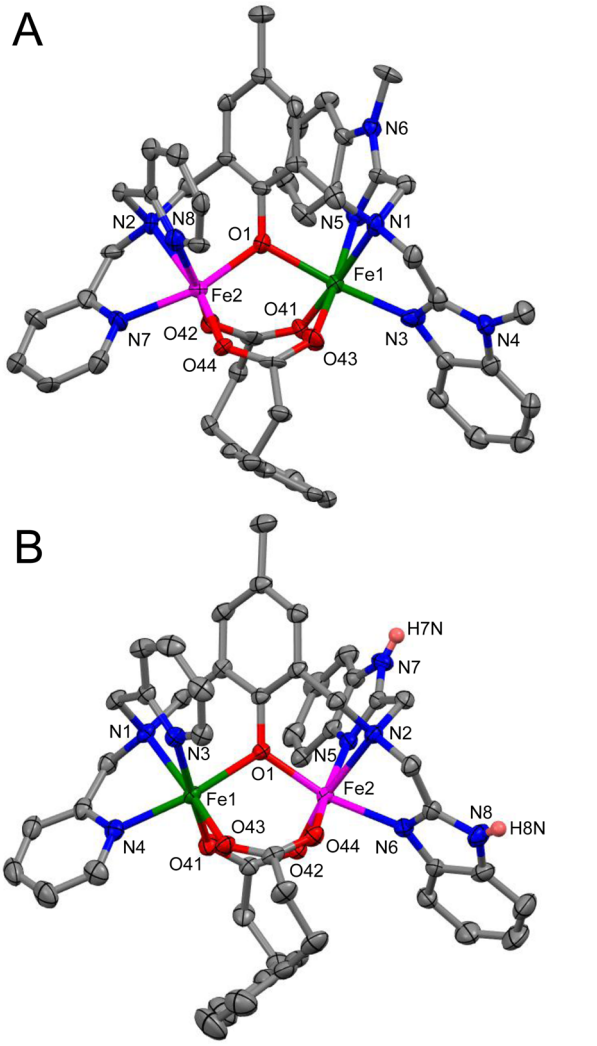

Figure 1. ORTEP drawing[22] of the dicationic complexes **3** (part A) and **4** (part B) with thermal ellipsoids drawn at the 50% probability level. Only the hydrogen atoms bound to the nitrogen atoms of the 1*H*-benzimidazole rings in **4** are shown. The Fe^{II} and Fe^{III} ions are drawn in green and pink, respectively.

Table 1. Fe−O1 and Average Fe−Ligand Bond Lengths (in Å) in 3 and 4

	Fe1−O1	average Fe1−L	Fe2−O1	average Fe2−L
3	2.127(5)	2.157	1.944(5)	2.064
4	2.0745(18)	2.122	1.9588(17)	2.069

ppm domain. They are reminiscent of those reported for analogous mixed-valent $Fe^{II}Fe^{III}$ species with high-spin iron ions. The first notable feature is the observed full spectral range: 340, 370, 365, 510, 435, and 380 ppm for complexes **2** to **7**, respectively. With the exception of complex **5**, the relatively narrow spectral range (390 ± 50 ppm) is similar to that observed in $[(bpmp)Fe_2(\mu\text{-}OPr)_2]^{2+}$ (390 ppm)[20] and $[(bimp)Fe_2(\mu\text{-}OAc)_2]^{2+}$ (350 ppm)[21] and indicates that the iron valences are delocalized (at least partly) on the NMR time scale. It has been previously demonstrated that the equatorial methylene protons of the binucleating ligands are detected above 150 ppm in $[(bpmp)Fe_2(\mu\text{-}OPr)_2]^{2+}$[20] and $[(bimp)\text{-}Fe_2(\mu\text{-}OAc)_2]^{2+}$.[21] Six such protons are present in **2**, but only three peaks are detected at 338, 199, and 170 ppm. This is fully

DOI: 10.1021/acs.inorgchem.5b00449
Inorg. Chem. 2015, 54, 6257−6266

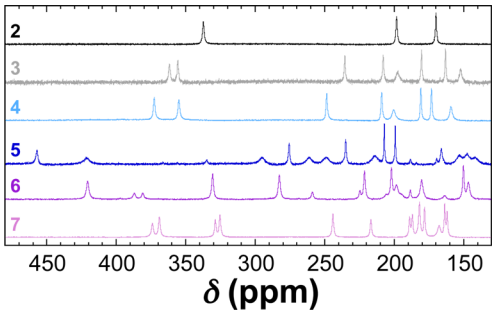

Figure 2. Four hundred eighty to 130 ppm domain of the ^{1}H NMR spectra of complexes **2**–**5** and **7** recorded in CD_3CN solutions and in the CD_3CN/d_7-DMF solution for complex **6**.

consistent with the delocalization of the iron valences. For **3** and **4**, owing to the asymmetry of the ligand, the methylene groups are nonequivalent, and indeed, six peaks are observed above 140 ppm that can be associated with the equatorial methylene protons.

By contrast, the larger spectral width observed for **5** is similar to that observed in **1** (ca. 550 ppm)[6,17] and in $[(L\text{-}Bn)Fe_2(\mu_2\text{-}mpdp)(S)]^{2+}$ (HL-Bn = 2-(*N*,*N*-bis((pyridin-2-yl)methyl)-aminomethyl)-6-(*N*-((pyridin-2-yl)methyl)-*N*-((benzyl)-aminomethyl)-4-methylphenol, S = CH_3CN or H_2O, 605 ppm),[18,19] indicating localized iron valences. The spectrum of **5** is indeed strongly reminiscent of that recorded in the ≈65:35 cis/trans isomer mixture of **1** (see Supporting Information Figure S3).[17] It is worth noticing that an intense and narrow peak is detected at −17 ppm for **5**. A similar signal was observed at −19 ppm for **1** that was indeed characteristic of the cis-isomer. Hence, the ^{1}H NMR spectrum of **5** reveals the coexistence of two isomers that, by analogy with **1**, we assign to the cis and trans coordination of the aniline with respect to the phenoxido bridge, the aniline being bound to the Fe^{II} site in **5**. Since the methylene protons in the trans-isomer of **1** are associated with the narrowest peaks (see Supporting Information, Figure S3), the same hypothesis applied to **5** allows one to estimate the cis/trans ratio to approximately 55:45. Thus, the cis-isomer is the major species in the two aniline complexes **1** and **5**.

For complexes **6** and **7**, the high number of peaks detected above 130 ppm also suggests the presence of two isomers, the 1*H*-benzimidazole ligand being cis or trans to the bridging phenoxide. The isomer ratio is close to 75:25 for **6** and to 60:40 for **7**, but we have no indication so far to assert if it corresponds to the cis/trans or trans/cis ratio. As mentioned above, the spectral ranges suggest that **6** and **7** have delocalized iron valences, the delocalization being more important in **7** than in **6**. The same trend is observed when comparing **5** and **1** that have the same nonprotic triamine branches, respectively. Remarkably, these ^{1}H NMR studies thus show that complexes **1**–**7** exhibit a complete range of electronic (de)localization of the Fe valences depending on the various combinations of amine ligands (see below).

UV–Visible Studies of Complexes 2–7. The UV–visible absorption spectra were recorded for complexes **2**–**7** and are shown in Supporting Information, Figure S4. As expected, the six complexes present a phenoxide-to-Fe^{III} charge transfer band in the 500–600 nm region (ε = 645–1365 M^{-1} cm^{-1}).

Mössbauer Studies of Complexes 2–7. To further characterize the complexes and to get more insights into the coordination spheres of the iron sites, we turned to Mössbauer spectroscopy. Mössbauer spectra were recorded at 80 K on powder samples for complexes **2**, **3**, and **5** and on solutions for complexes **4**–**7** (see Supporting Information, Figures S5 and S6, respectively). DMF was added for the complete dissolution of **6**. All spectra can be successfully simulated by assuming two doublets of equal area. The nuclear parameters are listed in Table 2. The isomer shift and quadrupole splitting values are similar to that observed for similar complexes and are fully consistent with a $Fe^{II}Fe^{III}$ composition, the two iron ions being in the high-spin state. The iron valences are thus localized at low temperatures. These simulations do not evidence the presence of cis/trans mixtures for complexes **5**–**7**. The two isomers are expected to differ mainly in the quadrupole splitting of the Fe^{II} site as in **1**.[17] However, the large line width of the ferrous site ($\Gamma_{fwhm} \geq 0.50$ mm/s) in **5**–**7** may hide the presence of such a mixture.

Table 2. Isomer Shift (δ) and Quadrupole Splitting (ΔE_Q) Values Used to Reproduce the 80 K Mössbauer Spectra of Complexes 2–7[a]

complex		δ (mm/s)	ΔE_Q (mm/s)	Γ_{fwhm} (mm/s)[b]
2[c]	Fe^{II}	1.16	2.69	0.30
	Fe^{III}	0.46	0.31	0.32
3[c]	Fe^{II}	1.16	2.90	0.33
	Fe^{III}	0.46	0.33	0.39
4[d]	Fe^{II}	1.12	2.64	−0.53
	Fe^{III}	0.47	0.51	0.41
5[c]	Fe^{II}	1.07	2.19	−0.71
	Fe^{III}	0.43	0.37	0.34
5[d]	Fe^{II}	1.16	2.60	0.56
	Fe^{III}	0.47	0.42	0.36
6[d]	Fe^{II}	1.16	2.60	0.50
	Fe^{III}	0.46	0.44	0.37
7[d]	Fe^{II}	1.16	2.68	0.54
	Fe^{III}	0.46	0.36	0.36

[a]Each iron site accounts for 50% of the total area. [b]The positive and negative signs correspond to Lorentzian and pseudo-Voigt profiles, respectively. [c]Recorded on a powder sample. [d]Recorded on frozen solutions.

Electrochemical Studies of Complexes 2–7. Cyclic voltammograms were recorded on millimolar CH_3CN solutions of complexes **2**–**7**. They are shown in Supporting Information, Figure S7. They all present two quasi-reversible waves associated with the metal centered one-electron reduction and one-electron oxidation of the mixed valence complexes generating the corresponding diferrous and diferric species (Chart 2).

Chart 2

$$[Fe^{II}(LH)Fe^{II}]^+ \underset{}{\overset{E_{red}^{1/2}}{\rightleftharpoons}} [Fe^{II}(LH)Fe^{III}]^{2+} + e^-$$

$$[Fe^{II}(LH)Fe^{III}]^{2+} \underset{}{\overset{E_{ox}^{1/2}}{\rightleftharpoons}} [Fe^{III}(LH)Fe^{III}]^{3+} + e^-$$

The values of the redox potentials are listed in Table 3. The two redox processes are separated by ≈700 mV, a value commonly determined for similar complexes.[15,21,23,24] The isomers detected by ^{1}H NMR for complexes **5**–**7** appear to behave identically in cyclovoltammetry. The values for complex **2** are higher than those of $[(bimp)Fe_2(\mu\text{-}OAc)_2]^{2+}$ and lower

DOI: 10.1021/acs.inorgchem.5b00449
Inorg. Chem. 2015, 54, 6257–6266

Table 3. Redox Potentials (in V vs SCE) in Increasing Order for Complexes 1−7 and Two Related Complexes

complex	ligands on the tertiary amines[a]		$E_{red}^{1/2}$	$E_{ox}^{1/2}$	ref
$[(bimp)Fe_2(\mu\text{-}OAc)_2]^{2+}$	$MeIm_2$	$MeIm_2$	−0.22	0.44	21
2	$MeBzIm_2$	$MeBzIm_2$	−0.18	0.52	this work
7	$MeBzIm_2$	Py/HBzIm	−0.15	0.54	this work
4	Py_2	$HBzIm_2$	−0.14	0.58	this work
3	Py_2	$MeBzIm_2$	−0.12	0.58	this work
5	$MeBzIm_2$	$Py/PhNH_2$	−0.09	0.62	this work
6	Py_2	Py/HBzIm	−0.09	0.63	this work
$[(bpmp)Fe_2(\mu\text{-}OPr)_2]^{2+}$	Py_2	Py_2	−0.01	0.69	20
1	Py_2	$Py/PhNH_2$	0.00	0.70	9

[a]The ligands are connected to the tertiary amines by a CH_2 group at position 2.

than those of $[(bpmp)Fe_2(\mu\text{-}OPr)_2]^{2+}$. As expected, values for **3** are in between those of **2** and those of $[(bpmp)Fe_2(\mu\text{-}OPr)_2]^{2+}$. This ordering is in agreement with the lower donating character of pyridine compared to that of 1-methylbenzimidazole. Comparison of these redox potentials for pairs of complexes confirms the expected trends and allows one to quantify them. Substituting the BPA complexing arm by BMBA leads to a decrease of the redox potentials in **5** and **7** compared to those in **1** and **6** (ca. −80 and −60 mV, respectively). Similarly, replacing the aniline by the 1*H*-benzimidazole facilitates oxidation according to the ca. 80 and 60 mV, respective, potential decrease measured in **6** and **7** versus **1** and **5**.

Deprotonation Studies of Complexes 4−7. The deprotonation by triethylamine was investigated for complexes **4**−**7** that contain a protic ligand, aniline for **5**, and 1*H*-benzimidazole for **4**, **6**, and **7**. The process was evidenced first by UV−visible spectroscopy and cyclic voltammetry and further studied by ^{1}H NMR and Mössbauer spectroscopies to get an insight into the possible formation of isomers as for **1**. The deprotonated complexes will be denoted **4′**−**7′**.

UV−Visible Studies of Complexes 4′−7′. Figure 3 displays the titrations of **5** and **7** by NEt_3, while those of **4** and **6** are reproduced in Supporting Information, Figure S8. Addition of NEt_3 induces an increase in the absorption that maximizes at titration completion at 728 nm for **5′** (ε_{728} = 4650 M^{-1} cm^{-1}), 532 nm for **4′** (ε_{532} = 3355 M^{-1} cm^{-1}), and 528 nm for **6′** (ε_{528} = 3330 M^{-1} cm^{-1}) and **7′** (ε_{528} = 3875 M^{-1} cm^{-1}). These four transformations occur with at least one isosbestic point, in agreement in every case with the presence of only two chromophores. The titration of **5** is reminiscent of that of **1**,[6] suggesting that **5′** is the mixed-valent $Fe^{II}Fe^{III}$ complex with the anilide coordinated to the ferric site. As in **1**, deprotonation of the aniline in **5** must have induced a valence inversion (see Scheme 1). The similarity of the absorption spectra recorded at titration completion for **4**, **6**, and **7** strongly suggests that the addition of NEt_3 leads to the deprotonation of the 1*H*-benzimidazole. As the anilide ligand is coordinated to the Fe^{III} ion in **1′** and **5′**, it is reasonable to propose that the generated benzimidazolide binds the ferric ion

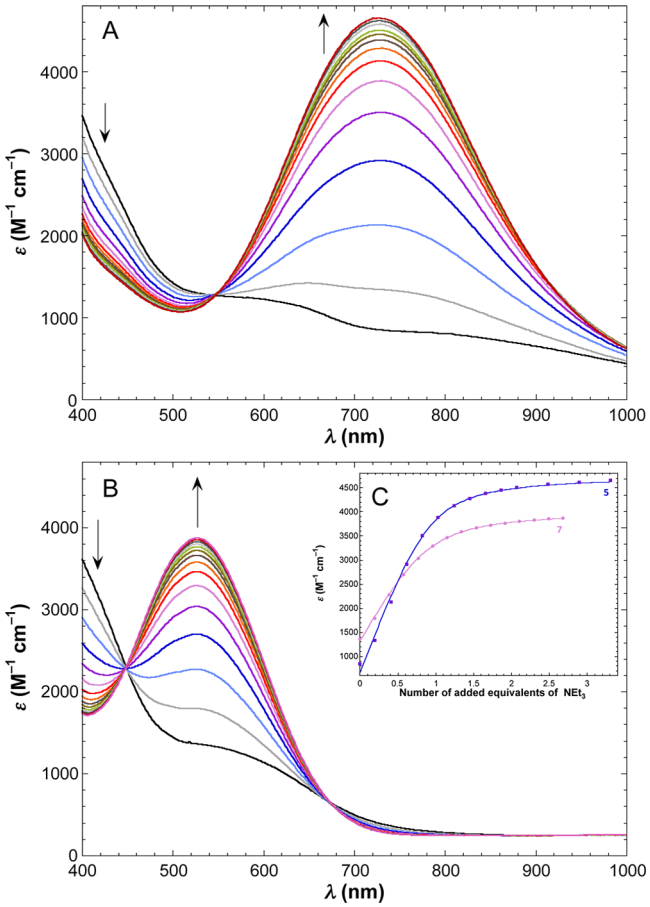

Figure 3. Titrations of **5** (part A) and of **7** (part B) in CH_3CN by NEt_3. The dependences of the absorption at 728 nm for **5** (dark blue squares) and at 528 nm for **7** (mauve dots) on the number of equivalents of the base are reproduced in part C. The best fits (solid lines, see text) obtained according to equation S2 (Supporting Information) lead to K_{app} = 12 ± 4 and 8.5 ± 1 for **5** and **7**, respectively.

in **4′**, **6′**, and **7′**. This will be further confirmed by ^{1}H NMR studies (see below). We propose this intense 530 nm absorption to correspond to a benzimidazolide-to-Fe^{III} charge transfer transition.

The variations of the absorption with the added equivalents of base can be satisfyingly reproduced by assuming the presence of two chromophores, the first corresponding to the acid form, and the second to the basic one, that are in equilibrium owing to the presence of NEt_3 and of its conjugated acid Et_3NH^+ (see Chart 3). The simulations lead to K_{app} = 4.8 ± 1, 12 ± 4, 7.5 ± 1, and 8.5 ± 1 for complexes **4** to **7**, respectively (see Supporting Information for the theoretical expressions). Complexes **1** and **5** bearing an aniline ligand are more acidic (K_{app} = 34 for **1**)[17] than complexes **4**, **6**, and **7** containing the 1*H*-benzimidazole ligand. These latter complexes present very similar K_{app} constants, suggesting that they are associated with

Chart 3. Definition of the K_{app} Constant Associated with the Deprotonation of 4−7 by NEt_3

$$[Fe^{II}(LH)Fe^{III}]^{2+} + NEt_3 \overset{K_{app}}{\rightleftharpoons} [Fe^{II}(L)Fe^{III}]^{+} + Et_3NH^{+}$$

4-7 **4′-7′**

DOI: 10.1021/acs.inorgchem.5b00449
Inorg. Chem. 2015, 54, 6257−6266

the same reaction, the deprotonation by NEt_3 of the 1*H*-benzimidazole ligand.

Electrochemical Studies of Complexes 4′−7′. Figure 4 reproduces the variations of the cyclovoltammograms of **5** and

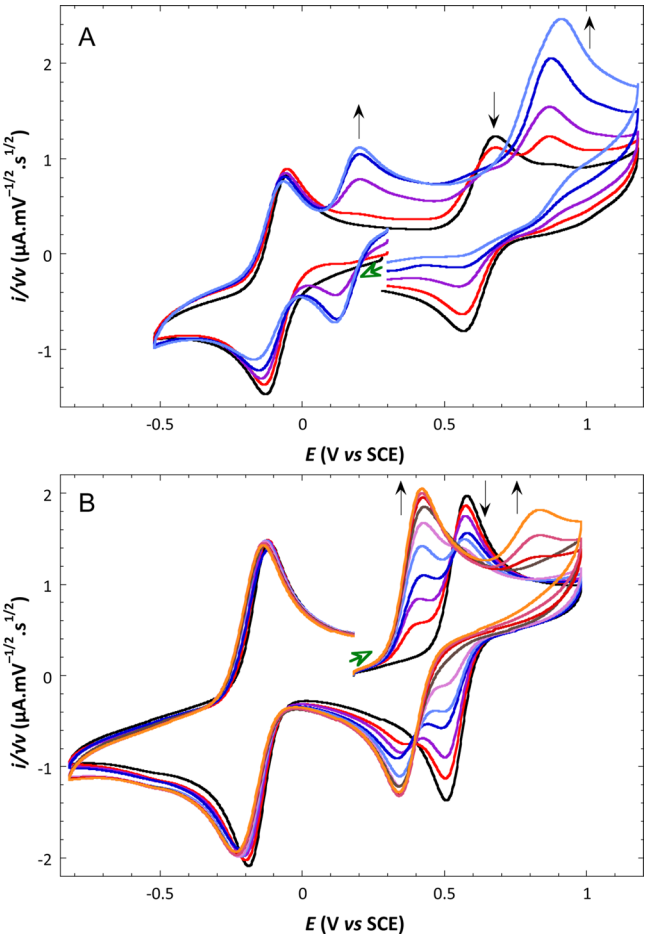

Figure 4. Dependence of the cyclic voltammograms of **5** (part A) and **7** (part B) upon the addition of increasing amounts of NEt_3 (0, 0.5, 1.0, 1.5, and 2.1 equiv for **5** and 0 to 0.94 equiv by 0.1 for **7**). The unfilled green arrow indicates the scan direction. The 0.87 V peak corresponds to the oxidation of excess NEt_3.

7 upon the addition of NEt_3. The analogous experiments with **4** and **6** are shown in Supporting Information, Figure S9. The main feature is the decrease of the wave associated with the oxidation process to the benefit of a new quasi-reversible wave detected at a lower potential. This new process may be associated with the one-electron oxidation of the deprotonated complexes **4′−7′** into diferric species (Chart 4). The associated redox potentials are listed in Table 4.

Chart 4

$$[Fe^{II}(L)Fe^{III}]^{+} \underset{}{\overset{E_{ox}^{1/2}}{\rightleftharpoons}} [Fe^{III}(L)Fe^{III}]^{2+} + e^{-}$$

For **5**, with an aniline ligand, the deprotonation leads to a 0.46 V decrease of the oxidation potential that is identical to that observed for **1**. For **4**, **6**, and **7**, this decrease is smaller, ca. 0.2 V. By contrast, for all complexes, the reduction to the diferrous state is essentially unaffected by the pH increase,

Table 4. Oxidation Potential (in V vs SCE) in Increasing Order for Complexes 1′ and 4′−7′

complex	ligands on the tertiary amines[a]		$E_{ox}^{1/2}$	ref
5′	$MeBzIm_2$	$Py/PhNH^-$	0.16	this work
1′	Py_2	$Py/PhNH^-$	0.24	9
4′	Py_2	$HBzIm/BzIm^-$	0.34[b]	this work
7′	$MeBzIm_2$	$Py/BzIm^-$	0.38	this work
6′	Py_2	$Py/BzIm^-$	0.46	this work

[a]The ligands are connected to the tertiary amines by a CH_2 group at position 2. [b]Value corresponding to the average of the anodic and cathodic peak values. The shape of the cyclovoltammograms indicates a slow electron transfer at the electrode.

suggesting that the deprotonated diferrous species are unstable and immediately (re)protonate as observed for **1′**.[9]

^{1}H NMR Studies of Complexes 4′−7′. To further characterize the deprotonated complexes **4′−7′**, we turned to ^{1}H NMR spectroscopy that was the single technique able to differentiate the isomers in the parent complexes **5**−**7**. The spectra of **4′−7′** are consistent with mixed-valent $Fe^{II}Fe^{III}$ species with high-spin ferrous and ferric ions. The spectrum of **5′** is very similar to that of **1′** (see Supporting Information, Figure S10). It expands over ca. 760 ppm, from 524 to −238 ppm, indicating that the iron valences are localized on the NMR time scale. In addition, two signals are detected at −208 and −238 ppm. They are the signatures of the two ortho protons of the anilide ring coordinated to the Fe^{III} site.[6,17] The close resemblance of the spectra of **5′** and **1′** strongly suggests that the trans-isomer is also the overwhelming species for **5′**: the anilide in trans position versus the phenoxido bridge is strongly favored. In the present case, the cis−trans isomerization reaction in **5′** is too fast to be monitored, and the proportion of the cis-isomer is too low to allow the identification of its NMR signature.

Figure 5A reproduces the evolution of the ^{1}H NMR spectra of a CD_3CN solution of **4** in the 540−80 ppm domain upon the addition of NEt_3 (see Supporting Information Figure S11 for the 145 to −30 ppm domain of the spectra). The spectrum recorded at completion (see spectrum (g) in Figure 5A) expands over ca. 515 ppm from 490 to −23 ppm. This suggests that the iron valences are localized in **4′** on the NMR time scale. We propose that the localization of the iron valences is induced by the deprotonation, the generated benzimidazolide being coordinated to the ferric ion. The variation of the position of six peaks attributed to equatorial or axial H nuclei of methylene groups (signals labeled A−D, F, and J in Figure 5A) of the dinucleating ligand in **4** are shown in Figure 6A. These six curves can be perfectly reproduced assuming a unique constant K_{app} (see Chart 3). The best fit leads to $K_{app,\,4} = 10 \pm 6$. This value also leads to a satisfying reproduction of the variations of four other signals (see Supporting Information, Figure S12). This value is consistent albeit larger with that determined from UV−visible studies. From the analogy of the spectrum of **4′** with that of $[Fe^{II}(L)(\mu\text{-}O_2P(OPh)_2)_2Fe^{III}]^+$ (H_2L = 2-(*N*,*N*-((pyridin-2-yl)methyl)aminomethyl)-6-(*N*-((pyridin-2-yl)methyl)-*N*-((2-hydroxyphenyl)methyl)aminomethyl)-4-methylphenol), we tentatively assign the most downfield shifted A−C signals in **4′** to the equatorial H protons of the methylene groups located on the ferric side, signal A originating from $N-CH_2-PhO^-$. The overall low number of resonances is inconsistent with the expected coexistence in solution of the cis- and the trans-isomers

DOI: 10.1021/acs.inorgchem.5b00449
Inorg. Chem. 2015, 54, 6257−6266

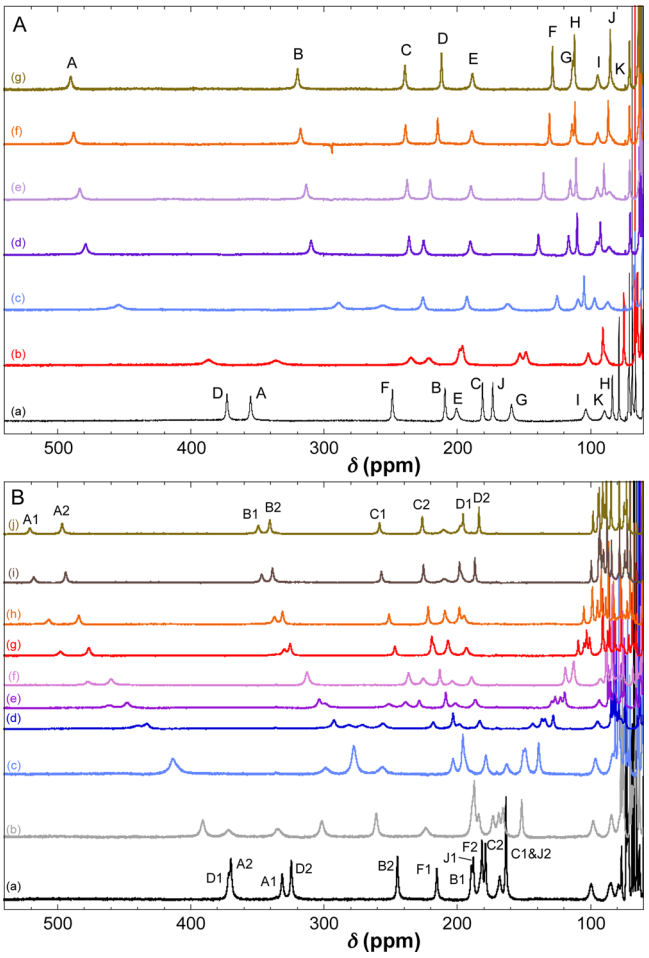

Figure 5. Evolution of the ^{1}H NMR spectra in the 550−80 ppm domain upon addition of increasing amounts of NEt_3 to CD_3CN solutions of **4** (part A) and **7** (part B). The numbers of added equivalents of base are for **4** (a) 0, (b) 0.30, (c) 0.90, (d) 1.50, (e) 1.80, (f) 2.26, and (g) 3.01 and for **7** (a) 0, (b) 0.21, (c) 0.41, (d) 0.62, (e) 0.82, (f) 1.03, (g) 1.54, (h) 2.06, (i) 4.12, and (j) 6.18.

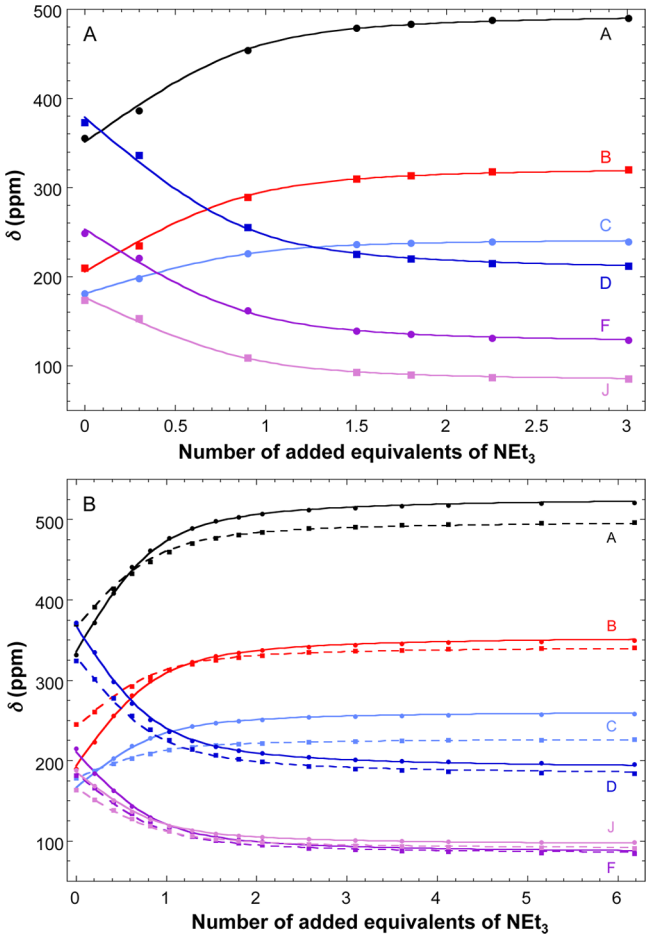

Figure 6. Dependence of a selection of NMR signals of **4** (part A) and **7** (part B) upon the addition of NEt_3. The labels of the signals refer to that in Figure 5. The solid and dotted lines reproduce the best fits obtained according to equation S10 (Supporting Information) with K_{app} = 10 ± 6 for **4** and 6.1 ± 1.5 for **7**. In part B, the closed circles and solid lines are associated with the signals of isomer 1 and the closed squares and dotted lines to those of isomer 2.

which should result from the deprotonation of a single 1*H*-benzimidazole group. This contradiction can be resolved if one considers that the two isomers differ only by a single proton bound to the *cis*- or *trans*-benzimidazole group. It is conceivable that this proton may exchange between the 1*H*-benzimidazole and the benzimidazolide groups rapidly on the NMR time scale, thus averaging the number of peaks (see Supporting Information, Scheme S3).

Similar NMR titration experiments were performed on **6** and **7**. The full-scale spectra are shown in Supporting Information, Figures S13 and S14, respectively. Figure 5B focuses on the 520−80 ppm window for the titration of **7**. As previously observed for the titration of **4**, the spectra at completion expand over a large width, ca. 515 ppm for the CD_3CN/d_7-DMF solution of **6′** and ca. 550 pm for the CD_3CN solution of **7′**. The deprotonated species thus present iron valences localized on the NMR time scale. As for **4′**, the localization of the iron valences would originate from the deprotonation, and we propose that the benzimidazolide is coordinated to the Fe^{III} ion in **6′** and **7′**. The comparison between the spectrum (g) of **4′** in Figure 5A on the one hand and spectrum (j) of **7′** in Figure 5B or spectrum (i) of **6′** in Supporting Information, Figure S14 on the other hand evidences a doubling of the signals in **7′** and **6′** vs **4′**. This suggests that **6′** and **7′** exist in solution as cis- and trans-isomers with distinctive NMR signatures. Assuming that the two most downfield signals of **6′** and **7′** located above 450 ppm are associated with the same proton but in different isomers, we estimate the isomer 1/isomer 2 ratio to be close to 30:70 in **6′** and 40:60 in **7′**. The presence of d_7-DMF for the complete dissolution of **6** leads to peak broadening, thus preventing a thorough analysis of the titration experiment. Consequently, we will focus here on the titration of **7**. By analogy with **4′**, the equatorial H nuclei of methylene groups of the binucleating ligand on the ferric side in **7′** would correspond to signals A1−C1 (respectively A2−C2) for isomer 1 (respectively isomer 2), with signals A1 and A2 corresponding to the $N-CH_2-PhO^-$ group. Figure 6B reproduces the evolution of the peak position for 12 signals, 6 for each isomer. These evolutions indicate that the isomer ratio remains constant during titration. Accordingly, the simultaneous fit of the 12 curves in Figure 6B led to $K_{app,\ 7}$ = 6.1 ± 1.5, in agreement with the above UV−visible investigations (see Supporting Information for theoretical equations). This analysis is further confirmed by the fit of the variation of the peak position of other protons (see Supporting Information, Figure S15). A definite assignment of a set of

DOI: 10.1021/acs.inorgchem.5b00449
Inorg. Chem. 2015, 54, 6257−6266

resonances to the cis- or trans-isomer is not possible since the benzimidazolide group lacks typical signatures as found in anilide[6,17] or phenoxide[10] terminal ligands in the trans-isomer of $Fe^{II}Fe^{III}$ complexes.

Mössbauer Studies of Complexes 4′−7′. NMR spectroscopy allows the distinction of the two isomers in **7′** and **6′**, and the identification of the single one in **5′** as the trans-isomer. To further characterize these isomers, we recorded Mössbauer spectra on solutions at the end of the titration for the four complexes **4**−**7**. 80 K Mössbauer spectra of **4′**−**7′** are reproduced in Supporting Information, Figure S16. These four spectra can be simulated with two doublets of equal area. The nuclear parameters are listed in Table 5. The isomer shift values are perfectly consistent with a mixed-valent composition with Fe^{II} and Fe^{III} ions in the high-spin state, in agreement with ^{1}H NMR studies. To the best of our knowledge, deprotonation of 1*H*-imidazole coordinated to Fe^{III} usually leads to low-spin ferric imidazolide species with the exception of $[Fe(Ph\text{-}Himap)_2]^+$ where the Fe^{III} remains high-spin in [Fe(Ph-Himap)(Ph-imap)] (Ph-Himap = 4-(2-hydroxyphenylimino-methyl)-2-phenylimidazole).[25] The main difference between complexes **4′**−**7′** is the quadrupole splitting value of the ferric site. We and others have previously evidenced that $[Fe^{II/III}(\mu\text{-}OR)(\mu\text{-}O_2X)_2Fe^{III}]^{2+/3+}$ complexes (RO^- = alkoxido or phenoxido, XO_2^- = carboxylato or phosphato) containing an additional negatively charged ligand on the ferric site in trans position with respect to the phenoxido or alkoxido bridge exhibit unusually large quadrupole splitting values for the Fe^{III} ion.[6,17,18,26−30] Smaller values are measured for cis-isomers.[10,17,26,27,31,32] Accordingly, the values listed in Table 5 suggest that a single isomer is present at low temperature for **4′**−**7′**. It is the trans-isomer for **4′** and **5′**, while it is the cis-isomer for **6′** and **7′**. This conclusion is fully consistent with NMR studies for **5′**. By contrast, for **6′** and **7′**, two isomers were detected by NMR; it is thus possible that one isomer is favored during the sample cooling required for Mössbauer experiments.

Table 5. Isomer Shift (δ) and Quadrupole Splitting (ΔE_Q) Values Used to Reproduce the 80 K Mössbauer Spectra of Solutions of Complexes 4′−7′[a]

Complex		δ (mm/s)	ΔE_Q (mm/s)	Γ_{fwhm} (mm/s)[b]
4′	Fe^{II}	1.13	2.51	−0.54
	Fe^{III}	0.52	1.72	0.36
5′	Fe^{II}	1.21	2.90	−0.36
	Fe^{III}	0.51	1.58	0.38
6′	Fe^{II}	1.07	2.34	0.58
	Fe^{III}	0.46	0.52	0.50
7′	Fe^{II}	1.17	2.83	0.40
	Fe^{III}	0.46	0.51	0.41

[a]Each iron site accounts for 50% of the total area. [b]The positive and negative signs correspond to Lorentzian and pseudo-Voigt profiles, respectively.

DISCUSSION

The study of complex **1** enabled us to evidence a pH-controlled valence inversion involving first-row transition metal ions and two isomerization processes in dinuclear complexes. Modifications of the binucleating ligand allow the synthesis of a series of mixed-valent $Fe^{II}Fe^{III}$ complexes. NMR spectroscopy reveals delocalization of the iron valences to different extents and confirms the presence in solution of two forms as in **1**. Changing the protic ligand from aniline to 1*H*-benzimidazole leads to interesting modification of the redox behavior.

Two Forms Are the cis- and trans-Isomers. The NMR spectra recorded on solutions of complexes **5**−**7** are typical of mixed-valent $Fe^{II}Fe^{III}$ complexes with high-spin metal ions. The number of peaks is inconsistent with a single complex present in solution. We have previously demonstrated for complex **1** that the two forms in equilibrium do not correspond either to valence isomers or to substitution of the aniline by an acetonitrile or a water molecule but to isomers that differ in the cis or trans coordination of the aniline ligand bound to the Fe^{II} with respect to the phenoxido bridge. The similarity between spectra of **1** and **5** allows one to conclude that analogous isomers exist for **5**. The same arguments apply to the 1*H*-benzimidazole analogues, and consequently, the two forms detected for **6** and **7** also correspond to the cis- and trans-isomers, the isomerization involving the 1*H*-benzimidazole ligand. Addition of NEt_3 allows the generation of the deprotonated species **6′** and **7′** that clearly present a coordinated benzimidazolide. The in depth analysis of the NMR titration of **7** allows the determination of the equilibrium constant associated with the deprotonation of the two forms by NEt_3. No significant difference between them was evidenced, strongly suggesting that the resulting two forms of the deprotonated complex **7′** are also the cis- and trans-isomers.

Pyridine vs 1-Methylbenzimidazole. As indicated above, substitution of BPA by BMBA has little or no influence on the isomer ratio either in the protonated species, **1** vs **5** and **6** vs **7**, or in the deprotonated ones, **1′** vs **5′** and **6′** vs **7′**. Consequently, the acid strengths of **5** and **7** are nearly identical to that of **1** and **6**, respectively. The 0.4 difference in the pK_a unit for **1** and **5** determined from the UV−visible titrations is just slightly above the uncertainty of the measurements. Cyclic voltammetry studies performed on **5**−**7** and previously on **1** show that this substitution leads to a stabilization of the +III iron oxidation state. The same ca. 70 mV decrease in the redox potential of the $Fe^{II}Fe^{III}/Fe^{III}Fe^{III}$ couple is observed when comparing **1′** with **5′**, **6′** with **7′**, and **3** with **2**. This is fully consistent with the better donating character of the 1-methylbenzimidazole ligand compared to that of the pyridine.

Aniline vs 1*H*-Benzimidazole. Substituting the aniline group by the 1*H*-benzimidazole also leads to a stabilization of the +III oxidation state. Indeed, both the reduction and oxidation waves of the protonated complexes **1** and **5** are shifted by ca. 75 mV toward more negative potentials in **6** and **7** (see Table 3). Upon deprotonation, the potential of the oxidation couple is displaced toward lower values for these four complexes. It is worth noticing that the shift is more important for the aniline-based complexes **1** and **5** (ca. 460 mV) than for 1*H*-benzimidazole-based species **6** and **7** (ca. 160 mV). Accordingly, the oxidation processes of **6′** and **7′** are detected at potentials ca. 220 mV higher than those of **1′** and **5′**. Consequently, the bisferric complexes are more favored with anilide than with benzimidazolide ligand. In addition, the ca. 160 mV drop of the oxidation process in **6** and **7** upon deprotonation is smaller than the ca. 230 and 250 mV decrease observed in the dinuclear complexes $[(bpp)FeS_2Fe(dtbp)]^{2}$[−33,34] (bpp^- = phenyl-benzimidazol-benzimidazolide, $dtbp^{2-}$ = 2,2′-dithiolide-1,1′-biphenyl) and $[Fe_2S_2(^{Pr}bbim)(^{Pr}bbimH)]^{2}$[−35] ($^{Pr}bbimH_2$ = 4,4-bis(benzimidazol-2-yl)-heptane) where the metal ions are in a tetrahedral environment. It is roughly half the one that has been estimated from the

DOI: 10.1021/acs.inorgchem.5b00449
Inorg. Chem. 2015, 54, 6257−6266

conversion of mononuclear high-spin ferrous complexes with three imidazole ligands into mononuclear low-spin ferric complexes with three imidazolides (ca. 300 mV per proton release).[23,36,37] In the latter case, this difference may originate from the high-spin state of the Fe^{III} center in **6′** and **7′**.

Titrations monitored by UV−visible absorption spectroscopy have shown similar acidity for the three complexes **4**, **6**, and **7**. Using $pK_a(Et_3NH^+)$ = 18.6 in CH_3CN[38] and assuming a 7.5 pH unit decrease of the pK_a in water compared to that in acetonitrile,[39] one gets a value of 10.3 ± 0.1 for the pK_a of these three complexes in water. The 1*H*-benzimidazole ligand is less acidic by ca. 7 and 10 pK_a units in the mixed-valent complexes $[Fe_2S_2(^{Pr}bbim)(^{Pr}bbimH)]^{-}$[35] and $[(bpp)FeS_2Fe(dtbp)]^{2-}$,[33,34] respectively. It is also more basic, however, to a weaker extent than the imidazole ligand in the reduced Rieske protein.[16] The pK_a-value compares well with that of the 1H-imidazole ring determined for the microperoxidase 11 complex[40] and for the three successive deprotonations of mononuclear ferric complexes bearing three imidazoles.[23] It is also close to that determined for $[Co^{III}(en)_2(OH)(ImH)]^{2+}$ and similar complexes.[41] Titration of **5** leads to K_{app} = 12 and thus to a pK_a value of **5** in water close to 10.0. This value is just slightly above that previously determined for **1** (9.6).[9] Surprisingly, the four complexes **4**−**7** present similar acid strengths, whereas aniline is 14 orders of magnitude less acid than 1*H*-benzimidazole (pK_a = 30.6 for aniline and 16.4 for 1*H*-benzimidazole in DMSO).[42] It is well-known that coordination of a protic molecule to a transition metal ion increases its acidity by several orders of magnitude. For instance, the pK_as of $[Fe^{II}(OH_2)_6]^{2+}$ and $[Fe^{III}(OH_2)_6]^{3+}$ have been determined to 9.5 and 2.2, respectively.[43] Aniline is expected to present a behavior similar to that of water owing to the exchangeable proton bound in both cases to the atom coordinating the metal ion. This acidity enhancement is expected to be weaker for 1*H*-benzimidazole owing to the remote exchangeable proton.[44] Serendipitously, this dissimilarity in the nature of the exchangeable proton leads to comparable acid strengths in the mixed-valent complexes investigated here.

CONCLUSIONS

This work has allowed a comparison of the properties of aniline and 1*H*-benzimidazole as terminal ligands to an iron ion. Interestingly, 1*H*-benzimidazole stabilizes the $Fe^{III}Fe^{III}$ redox state by 75 mV with respect to aniline. However, in the deprotonated forms, the reverse is observed since anilide stabilizes the $Fe^{III}Fe^{III}$ redox state by 230 mV with respect to 1*H*-benzimidazolide. This inversion results from a larger stabilization of the $Fe^{III}Fe^{III}$ redox state by deprotonation of aniline (460 mV) with respect to 1*H*-benzimidazole (160 mV). This difference can have two origins: (i) the delocalization of the charge in benzimidazolide, which will lessen the interaction with the Fe^{III} ion and (ii) the ability of the anilide to engage in a six-membered ring by coordination to Fe^{III}, whereas 1*H*-benzimidazolide is restricted to a less flexible five-membered ring.

EXPERIMENTAL SECTION

General Methods. *Materials.* Acetonitrile for spectroscopic measurements was distilled under argon over CaH_2 and stored within an inert atmosphere glovebox. All other reagents were of reagent grade quality and used as received.

Physicochemical Studies. ^{1}H NMR spectra were recorded in deuterated acetonitrile on a Bruker AC 200 with a 5 mm indirect detection as described previously.[10] The elemental analyses have been performed in the Centre Régional de Mesures Physiques pour l'Ouest (University of Rennes 1, France) and at the Service de Microanalyse of the Département de Chimie Moléculaire (University of Grenoble-Alpes, France). Mass spectra were obtained in the electrospray ionization mode on a LCQ-Finnigan Thermoquest spectrometer equipped with an octupolar analyzer and an ion trap. Electronic absorption spectra were recorded in acetonitrile (0.1−0.2 mM solutions with 1 cm optical length cuvettes) on a Varian Cary 50 spectrometer. Mössbauer spectra were recorded on 2−4 mM solutions of nonenriched complexes except for **4** and **4′** that were fully ^{57}Fe-enriched. The experiments were performed using a horizontal transmission cryostat (Oxford Instruments) and a 50 mCi source of ^{57}Co(Rh) as previously described.[6] All velocity scales and isomer shifts are referred to metallic iron foil at room temperature. Analysis of the data was performed with the software WMOSS4Mossbauer Spectral Analysis Software; www.wmoss.org, 2012.

Diffraction data were taken using an Oxford-Diffraction XCalibur S kappa geometry diffractometer (Mo−Kα radiation, graphite monochromator, λ = 0.71073 Å). To prevent evaporation of cocrystallized solvent molecules, the crystals were coated with light hydrocarbon oil, and the data were collected at 150 K. The cell parameters were obtained with intensities detected on three batches of 5 frames. The crystal−detector distance was 4.5 cm. The number of settings and frames has been established taking in consideration the Laue symmetry of the cell by CrysAlisPro Oxford-diffraction software.[45] Four hunded ten for **3** and 498 for **4** narrow data were collected for 1° increments in ω with a 320 s exposure time for **3** and 50 s for **4**. Unique intensities detected on all frames using the Oxford-diffraction Red program[45] were used to refine the values of the cell parameters. The substantial redundancy in data allows empirical absorption corrections to be applied using the ABSPACK Oxford-diffraction program for both compounds.[45] Space groups were determined from systematic absences, and they were confirmed by the successful solution of the structure. The structures were solved by a charge flipping method using SUPERFLIP software.[46] All non-hydrogen atoms were found by and refined on F^2.[47] Hydrogen atoms were found by difference Fourier syntheses and refined for **3** and **4**, except for the hydrogen atoms of the acetonitrile methyl group which were fixed in ideal position and refined with a riding model.

Electrochemical measurements were carried out using a PAR model 273 potentiostat. All electrochemical experiments were run under an argon atmosphere in a glovebox, using a standard three-electrode electrochemical cell. All potentials were referred to a Ag/AgCl-(saturated) reference electrode in an acetonitrile/0.1 M tetra-*n*-butylammonium perchlorate (TBAP) electrolyte. The potential of the regular ferrocene/ferrocenium (Fc/Fc^+) redox couple used as an internal standard was 0.36 V under our experimental conditions. The working electrodes were platinum disks polished with 1 μm diamond paste that were 5 mm in diameter for cyclic voltammetry experiments.

ASSOCIATED CONTENT

Supporting Information

Description of the syntheses of the ligands and complexes; crystallographic data of **3** and **4**; and additional ^{1}H NMR, UV−visible, and Mössbauer spectra and cyclovoltammograms. The Supporting Information is available free of charge on the ACS Publications website at DOI: 10.1021/acs.inorgchem.5b00449.

AUTHOR INFORMATION

Corresponding Authors

*(G.B.) E-mail: genevieve.blondin@cea.fr.
*(J.-M.L.) E-mail: jean-marc.latour@cea.fr.

Present Addresses

#(E.G.) Univ. Grenoble Alpes, DCM/CIRE, 38041 Grenoble Cedex 9, France.

DOI: 10.1021/acs.inorgchem.5b00449
Inorg. Chem. 2015, 54, 6257−6266

▽(M.C.) CEA, ICSM/LHYS, Site de Marcoule, 30207 Bagnols sur Cèze, France.

Notes

The authors declare no competing financial interest.

■ ACKNOWLEDGMENTS

The Agence Nationale de la Recherche (Grants ANR 2010 BLAN 703 and ANR-11-LABX-0003-01) and the Région Rhône-Alpes (Grants CIBLE 07 016335 and CIBLE 08 019180) are gratefully acknowledged for their financial support.

■ REFERENCES

(1) Creutz, C.; Taube, H. *J. Am. Chem. Soc.* **1973**, *95*, 1086−1094.
(2) Aguirre-Etcheverry, P.; O'Hare, D. *Chem. Rev.* **2010**, *110*, 4839−4864.
(3) Ceccon, A.; Santi, S.; Orian, L.; Bisello, A. *Coord. Chem. Rev.* **2004**, *248*, 683−724.
(4) D'Alessandro, D.; Keene, F. R. *Chem. Rev.* **2006**, *106*, 2270−2298.
(5) Kaim, W.; Sarkar, B. *Coord. Chem. Rev.* **2007**, *251*, 584−594.
(6) Gouré, E.; Thiabaud, G.; Carboni, M.; Gon, N.; Dubourdeaux, P.; Garcia-Serres, R.; Clémancey, M.; Oddou, J.-L.; Robin, A. Y.; Jacquamet, L.; Dubois, L.; Blondin, G.; Latour, J.-M. *Inorg. Chem.* **2011**, *50*, 6408−6410.
(7) Neyhart, G. A.; Meyer, T. J. *Inorg. Chem.* **1986**, *25*, 4807−4808.
(8) McCormick, J. M.; Reem, R. C.; Solomon, E. I. *J. Am. Chem. Soc.* **1991**, *113*, 9066−9079.
(9) Balasubramanian, R.; Blondin, G.; Canales, J. C.; Costentin, C.; Latour, J.-M.; Robert, M.; Savéant, J.-M. *J. Am. Chem. Soc.* **2012**, *134*, 1906−1909.
(10) Lambert, E.; Chabut, B.; Chardon-Noblat, S.; Deronzier, A.; Chottard, G.; Bousseksou, A.; Tuchagues, J.-P.; Laugier, J.; Bardet, M.; Latour, J.-M. *J. Am. Chem. Soc.* **1997**, *119*, 9424−9437.
(11) Haga, M.-a.; Ali, M. M.; Koseki, S.; Fujimoto, K.; Yoshimura, A.; Nozaki, K.; Ohno, T.; Nakajima, K.; Stufkens, D. J. *Inorg. Chem.* **1996**, *35*, 3335−3347.
(12) Haga, M.-a.; Ano, T.-a.; Kano, K.; Yamabe, S. *Inorg. Chem.* **1991**, *30*, 3843−3849.
(13) Kobayashi, K.; Ishikubo, M.; Kanaizuka, K.; Kosuge, K.; Masoka, S.; Sakai, K.; Nozaki, K.; Haga, M.-a. *Chem.—Eur. J.* **2011**, *17*, 6954−6963.
(14) Dong, Y.; Ménage, S.; Brennan, B. A.; Elgren, T. E.; Jang, H. G.; Pearce, L. L.; Que, L., Jr. *J. Am. Chem. Soc.* **1993**, *115*, 1851−1859.
(15) Suzuki, M.; Oshio, H.; Uehara, A.; Endo, K.; Yanaga, M.; Kida, S.; Saito, K. *Bull. Chem. Soc. Jpn.* **1988**, *61*, 3907−3913.
(16) Hsueh, K.-L.; Westler, W. M.; Markley, J. L. *J. Am. Chem. Soc.* **2010**, *132*, 7908−7918.
(17) Gouré, E.; Carboni, M.; Dubourdeaux, P.; Clémancey, M.; Balasubramanian, R.; Lebrun, C.; Bayle, P.-A.; Maldivi, P.; Blondin, G.; Latour, J.-M. *Inorg. Chem.* **2014**, *53*, 10060−10069.
(18) Chardon-Noblat, S.; Horner, O.; Chabut, B.; Avenier, F.; Debaecker, N.; Jones, P.; Pécaut, J.; Dubois, L.; Jeandey, C.; Oddou, J.-L.; Deronzier, A.; Latour, J.-M. *Inorg. Chem.* **2004**, *43*, 1638−1648.
(19) Kanda, W.; Moneta, W.; Bardet, M.; Bernard, E.; Debaecker, N.; Laugier, J.; Bousseksou, A.; Chardon-Noblat, S.; Latour, J.-M. *Angew. Chem., Int. Ed. Engl.* **1995**, *34*, 588−590.
(20) Borovik, A. S.; Papaefthymiou, V.; Taylor, L. F.; Anderson, O. P.; Que, L., Jr. *J. Am. Chem. Soc.* **1989**, *111*, 6183−6195.
(21) Mashuta, M. S.; Webb, R. J.; McCusker, J. K.; Schmitt, E. A.; Oberhausen, K. J.; Richardson, J. F.; Buchanan, R. M.; Hendrickson, D. N. *J. Am. Chem. Soc.* **1992**, *114*, 3815−3827.
(22) Bruno, I. J.; Cole, J. C.; Edgington, P. R.; Kessler, M.; Macrae, C. F.; McCabe, P.; Pearson, J.; Taylor, R. *Acta Crystallogr., Sect. B* **2002**, *58*, 389−397.
(23) Lambert, F.; Policar, C.; Durot, S.; Cesario, M.; Yuwei, L.; Korri-Youssoufi, H.; Keita, B.; Nadjo, L. *Inorg. Chem.* **2004**, *43*, 4178−4188.
(24) Suzuki, M.; Uehara, A.; Oshio, H.; Endo, K.; Yanaga, M.; Kida, S.; Saito, K. *Bull. Chem. Soc. Jpn.* **1987**, *60*, 3547−3555.
(25) Okamura, S.; Maeda, Y. *J. Radioanal. Nucl. Chem.* **2003**, *255*, 523−528.
(26) Neves, A.; Erthal, S. M. D.; Drago, V.; Griesar, K.; Haase, W. *Inorg. Chim. Acta* **1992**, *197*, 121−124.
(27) Krebs, B.; Shepers, K.; Bremer, B.; Henkel, G.; Althaus, E.; Müller-Warmuth, W.; Griesar, K.; Haase, W. *Inorg. Chem.* **1994**, *33*, 1907−1914.
(28) Neves, A.; de Brito, M. A.; Drago, V.; Griesar, K.; Haase, W. *Inorg. Chim. Acta* **1995**, *237*, 131−135.
(29) Nie, H.; Aubin, S. M. J.; Mashuta, M. S.; Wu, C.-C.; Richardson, J. F.; Hendrickson, D. N.; Buchanan, R. M. *Inorg. Chem.* **1995**, *34*, 2382−2388.
(30) Neves, A.; de Brito, M. A.; Vencato, I.; Drago, V.; Griesar, K.; Haase, W.; Mascarenhas, Y. P. *Inorg. Chim. Acta* **1993**, *214*, 5−8.
(31) Campbell, V. D.; Parsons, E. J.; Pennington, W. T. *Inorg. Chem.* **1993**, *32*, 1773−1778.
(32) Avenier, F.; Gouré, E.; Dubourdeaux, P.; Sénèque, O.; Oddou, J.-L.; Pécaut, J.; Chardon-Noblat, S.; Deronzier, A.; Latour, J.-M. *Angew. Chem., Int. Ed.* **2008**, *47*, 715−717.
(33) Albers, A.; Bayer, T.; Demeshko, S.; Dechert, S.; Meyer, F. *Chem.—Eur. J.* **2013**, *19*, 10101−10106.
(34) Albers, A.; Demeshko, S.; Dechert, S.; Saouma, C. T.; Mayer, J. M.; Meyer, F. *J. Am. Chem. Soc.* **2014**, *136*, 3946−3954.
(35) Saouma, C. T.; Kaminsky, W.; Mayer, J. M. *J. Am. Chem. Soc.* **2012**, *134*, 7293−7296.
(36) Carina, R. F.; Verzegnassi, L.; Bernardinelli, G.; Williams, A. F. *Chem. Commun.* **1998**, 2681−2682.
(37) Brewer, C.; Brewer, G.; Luckett, C.; Marbury, G. S.; Viragh, C.; Beatty, A. M.; Scheidt, W. R. *Inorg. Chem.* **2004**, *43*, 2402−2415.
(38) Izutsu, K. In *Acid-Base Dissociation Constants in Dipolar Aprotic Solvents*; Blackwell Scientific Publications: Boston, MA, 1990; pp 17−35.
(39) Dubé, C. E.; Wright, D. W.; Armstrong, W. H. *J. Am. Chem. Soc.* **1996**, *118*, 10910−10911.
(40) Das, D. K.; Medhi, O. K. *J. Chem. Soc., Dalton Trans.* **1998**, 1693−1698.
(41) Brodsky, N. R.; Nguyen, N. M.; Rowan, N. S.; Storm, C. B.; Butcher, R. J.; Sinn, E. *Inorg. Chem.* **1984**, *23*, 891−897.
(42) Bordwell, F. G. *Acc. Chem. Res.* **1988**, *21*, 456−463.
(43) Huynh, M. H. V.; Meyer, T. J. *Chem. Rev.* **2007**, *107*, 5004−5064.
(44) Sundberg, R. J.; Martin, R. B. *Chem. Rev.* **1974**, *74*, 471−517.
(45) *CrysAlisPro Software System*; Agilent Technologies UK Ltd., Oxford, U.K.
(46) Palatinus, L.; Chapuis, G. *J. Appl. Crystallogr.* **2007**, *40*, 786−790.
(47) Sheldrick, G. M. *Acta Crystallogr., Sect. A* **2008**, *64*, 112−122.

DOI: 10.1021/acs.inorgchem.5b00449
Inorg. Chem. 2015, 54, 6257−6266